SERA
Seismology and Earthquake Engineering
Research Infrastructure Alliance for Europe

DELIVERABLE

D25.5 ESHM20: hazard, sensitivity analyses, disaggregation (update M36)

Work package	WP25
Lead	ETH
Authors	Laurentiu Danciu, ETH Zurich
Reviewers	-
Approval	Management Board
Status	Final
Dissemination level	Restricted to SERA participants until approved by EC
Delivery deadline	M24 - Updated M36
Submission date	30.04.2020
Intranet path	DOCUMENTS/DELIVERABLES/ SERA_D25.5_ESHM20_Hazard_Sensitivity_Disaggregation.pdf

This project has received funding from the European Union's Horizon 2020 research and innovation programme under grant agreement No 730900.

Table of Contents

Summary – Note to the Project Management and EC officer

This deliverable was shifted to M36 rather than the M24, due to a mutual agreement between the CEN/TC 250/SC 8 technical commission and SERA consortium. In this report we are summarizing the status of the seismogenic source model of the 2020 European Seismic Hazard Assessment. This report provides an update of latest development of the ESHM20, and at the time of reporting (April 2020) this report updates the SERA Deliverable D25.5. Note, the SERA Deliverable 25.3 and 25.4 have been alos updated. The seismogenic source models, as well as the ground motion models have been presented during four regional workshops in Lisbon (June, 6th to 7th ,2019), Potsdam, June (12th to 13th2019), Athens, July (2nd to 3rd). The first set of hazard estimates have been presented for the first time in during a joint workshop SERA-CEN SC8 in Pavia (October 14th, 2019). In this meeting it has been agreed the road map to release the ESHM20 in September 2020 at the 37th General Assembly (GA) of the European Seismological Commission in a special session. Thus, the agreement between CEN/TC250/SC8 and SERA representatives (see SERA Deliverable D2.14 - Stakeholders workshop M30) indicate the review schedule of the ESHM20 as following: alpha model in October 2020-, beta-model (pre-release model) in April 2020 (Annual Meeting of SERA) and the final model in mid 2020.

The alpha model is the first hazard model computed end to end with focus on analysis of the components, model integration, software development and incorporating the uncertainties of data and model. The model was based on the data compiled up to M24 of the project. The ESHM20 beta model is built upon data and models compiled until M35 of the project and it is the model that it is described in this deliverable. Furthermore, the beta-model will be submitted for review and feedback to the national experts and the scientific community in Spring 2020. Within the review process it shall be expected that the model will evolve until mid 2020, thus the current documentation will be augmented with the review feedback and/or recommendations. An accompanying report and a scientific (peer-reviewed) paper describing the final model in detail is planned beyond the end of the SERA Project (April 2020).

Disclaimer:

This deliverable it is not intended to be the documentation of the 2020 European Seismic Hazard Model; The deliverable summarizes the working progress and reports the status of activities within the reporting period M24 to M36 or the SERA Project. The content of this Deliverable is restricted to the use of the SERA participants.

1 Hazard Calculation

Computational of the seismic hazard for large-scale region, covering the entire Euro-Mediterranean region, including Turkey, is challenging both the seismic hazard modelers team and the IT developers' team. The main challenges are linked to the complexity of the seismogenic source model, the size of the region, as well as the complexity of the seismic hazard output: seismic hazard maps, hazard curves, uniform hazard spectra, and disaggregation of the ground motion estimates.

OpenQuake-engine (Pagani et al 2014) will be used for computing the seismic hazard for the ESHM20. The engine was used for the computation of the ESHM13, and it an open-source hazard and risk calculation engine developed by the Global Earthquake Model (GEM) initiative.

For computation of the ESHM13, we adopted the classical Probabilistic Seismic Hazard Analysis (PSHA) calculator that estimates the probabilities that various earthquake-induced ground motion levels will be exceeded at a given location in a given time period by solving the PSHA integration procedure (Pagani et al 2014). The workflow of earthquake hazard calculators integrated in the OpenQuake engine is given in Figure 1.

The key features of OpenQuake (here we refer to the hazard library as OQ-hazard engine) are the state-of-the art seismic source representation, advance treatment of uncertainties and various options for hazard calculators. We used the default seismic source definitions of OQ-hazard engine as the blueprints to design our source models; hence, individual sources were parameterized according to the User's Manual (Crowley et al., 2015). According to the software manual, geometry parameters and seismicity occurrence models represent each seismic source. The geometry implies definition of source location, style-of-faulting, and depth. In particular, for the area and point sources, the style of faulting is of significant importance.

The software allows defining extensive ruptures linked to the magnitude distribution; hence, a seismic source is not a point source when magnitude exceeds a certain threshold. In this calculation, the threshold is fixed to magnitudes greater then 5.7. The impact of using extensive ruptures on the hazard estimates regarding the point-rupture approximation, leads to a significant increase in the probabilities of exceedance for specific level of motion (Monelli et al., 2014). Moreover, sensitivity analysis on the impact of extensive ruptures to response spectra at long periods must be investigated.

Style-of-faulting of future earthquake ruptures is assessed source by source based on various data sets, including earthquake focal mechanisms, stress indicators, stress orientation and geological structure. Results of the assessment are relative frequency of strike-slip versus normal and reverse faulting averaged across each seismic source.

Style-of-faulting frequency values are treated as aleatory variability and converted to probabilistic weights for seismic hazard. Additional parameters are the lower and upper seismogenic depth describing the region where source specific extensive ruptures are allowed to propagate.

Crustal faults are modelled as simple faults, and the subduction interface zones are represented as complex faults. A simple fault describes a fault surface projected along strike and dip. A complex fault does not require a dip angle because the geometry can be described by combinations of fault edges to describe top, mid or bottom of a fault surface.

Common to all sources is the magnitude scaling relationship; the scaling relationship controls the size of floating ruptures as a function of magnitude. A truncated magnitude frequency distribution, defined by the activity parameters (a- and bGR-value), lower and upper magnitude is used to characterize all seismic sources.

Minimum magnitude used in the probabilistic hazard calculation is 4.5 Mw, whereas the upper bounds vary accordingly to the Mmax logic tree (see SERA Deliverable D25.3).

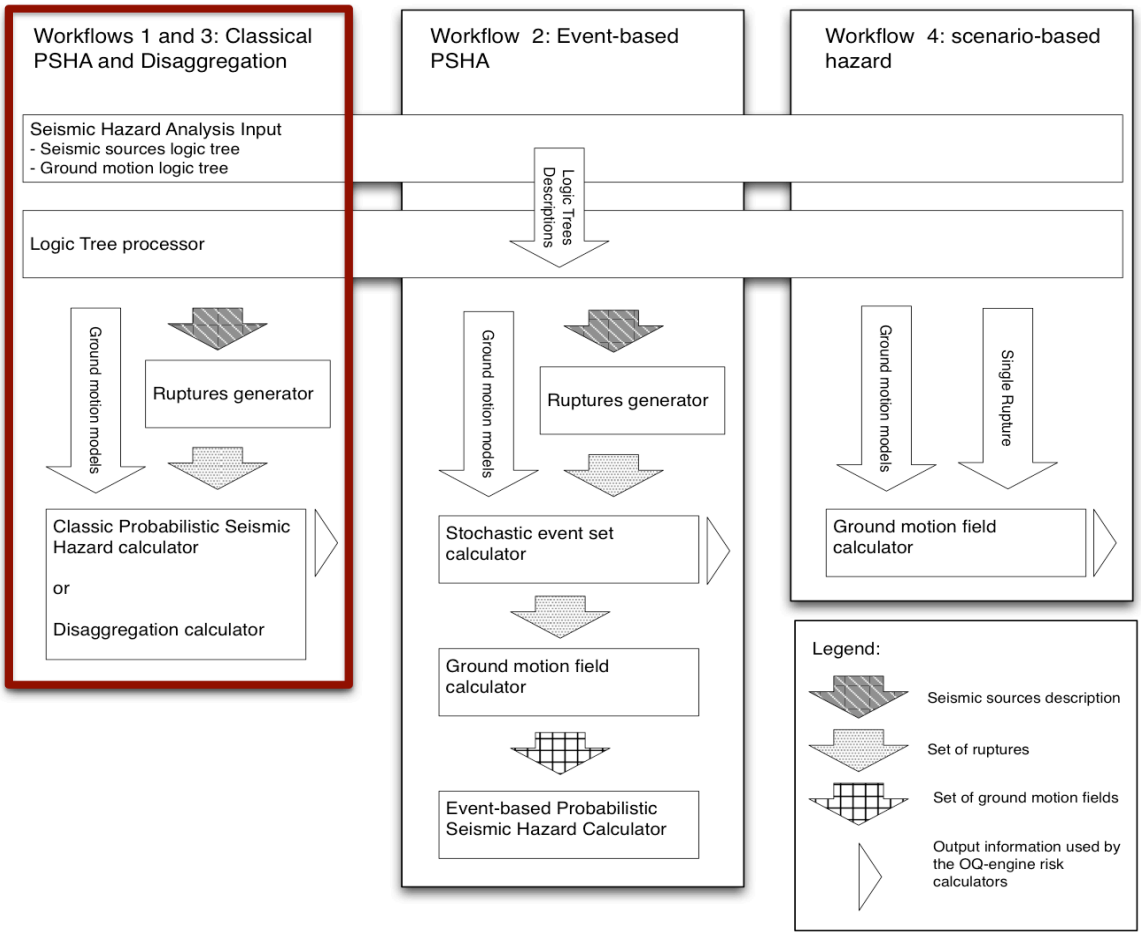

Figure 1 OpenQuake hazard engine modules and workflow. Red box highlights the procedure adopted for ESHM13 calculation (from OQ book)

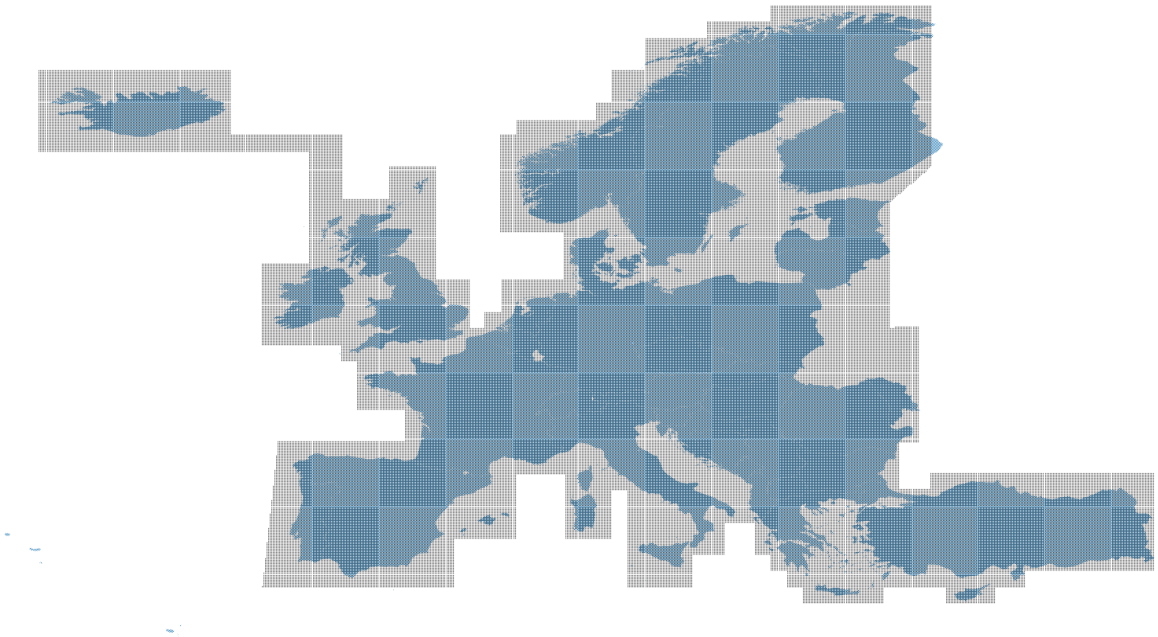

Figure 2 Computational grid for seismic hazard calculation of ESHM20 – the grid points are equally spaced at 0.1 to 0.1 degrees

2 ESHM20: Sensitivity Analyses

In this section we highlight some of the sensitivity analyses considered during the development of the seismic hazard model. Note that these analyses focus on various components of the model and aimed at supporting the experts in decision making.

2.1 Earthquake Catalogue: Completeness and Declustering

This section summarizes the sensitivity analyses conducted together with the statistical analysis of the earthquake unified earthquake catalogue. The main analyses are:

- Choice of declustering algorithm and the impact to regional seismic productivity
- Assessment of the uncertainties on the completeness estimates, time and magnitude of completeness
- Regional variability of the activity rates on super zones

The results are presented in the next sections.

2.1.1 Sensitivity analysis of the declustering methods:

We conducted a parameter sensitivity study for all declustering techniques considered by ESHM20. The parameters to be varied are listed in Table 2. We first considered the crustal part of the unified earthquake catalogue for ESHM20 as input for seismicity declustering. We define crustal seismicity as the part of the catalog that features depth values < 60km or (2) mapped NaN depth values. This definition leads to a total of 57480 crustal events.

We report a large variability in terms of number of mainshocks when comparing the different techniques. This variability is more dominant than the variability given by parameter changes for a single selected method (see Figures 11 and 12).

Thus, we selected three methods for further investigation with the default input parameters given in bold font in Table 2. The method that generates the largest number of events after declustering is the Reasenberg method with 48737 events identified as main events, followed by Zaliapin method with 33149 main events and default time windows technique used in ESHM with 23269 main events.

However, these results do not provide a straightforward answer in which method to be chosen. Thus, at a glance one could use the default time-window declustering technique, which was used in ESHM13. This method is was calibrated for the seismicity in central Europe, and it might provide an aggressive declustering as the number of events remaining is the lower among the considered declustering techniques.

A spatial comparison of the total number of events identified as mains by the three declustering methods is given in Figure 13. The comparison is done in grid cells of 50km and only events of magnitude greater than 4.5 are illustrated. It can be seen that when compared with the WT-

Grünthal the Reasenberg method identifies more main events in stable continental regions (Central Europe, Iberia, whereas in the southern Europe this trend is reversed.

On the same figure (bottom plot), the spatial comparison between the WT-Grünthal the Zaliapin method, suggests that the Zaliapin method might be suitable for very active regions (i.e. Southern Europe), as in the central Europe the number of main events identified are below the WT-Grünthal method. However, these are just some assumptions not supported by any other evidences, hence we progress with a data-driven procedure to aid the selection of the suitable declustering technique. A testing framework is provided in the next section.

Parameter	Description	Range/
fs_time_prop	fraction of the time window used for foreshocks	[1.0, 0.5, 0.1, **0.17**, 0.01,
taumin	Minimum look ahead time for clustered events	[1.0]
taumax	maximum look ahead time for clustered events	[**10.0**, 50.0 100 300] days
xmeff	effective magnitude to define magnitude cutoff (with	[**3.5**, 4.5, 5.5,
rfact	factor for interaction radius for dependent events	[**10.0**, 20.0 30.0]
fractal_dim	spatial weighting factor	[1.4, **1.6**, 1.8]
b_value	magnitude weighting factor	[0.9, **1.0**, 1.1]
theta	temporal weighting factor	[0.5, **1.0**, 2.0]

Table 2: Input parameters of the main declustering techniques under investigation for use in declustering the unified earthquake catalogue. The bolded parameters are considered as the reference input parameters.

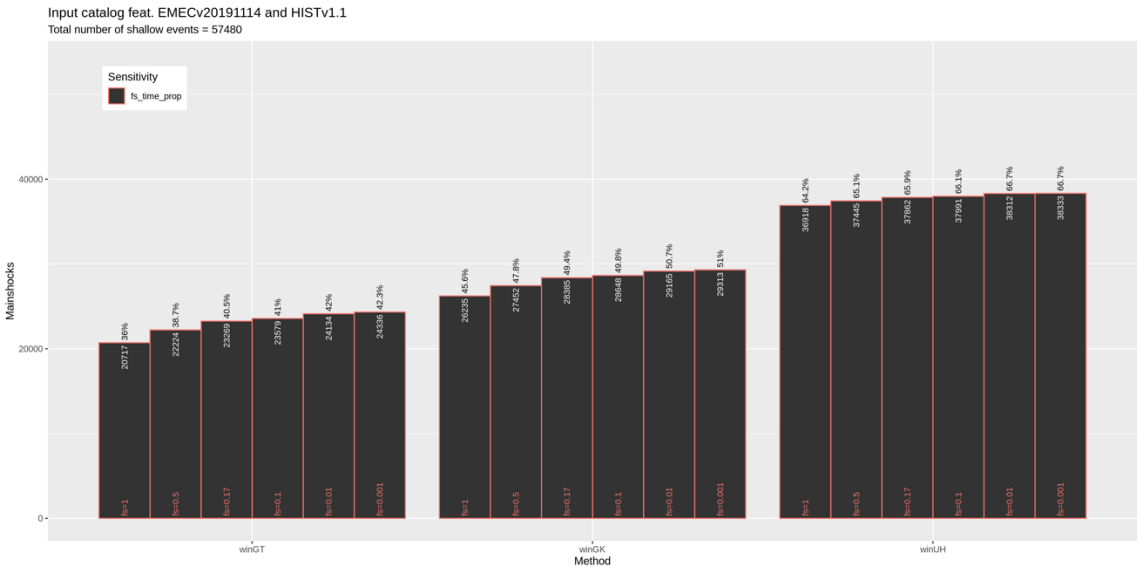

Figure 3: Parameter sensitivity overview for all conducted windowing declustering methods

(GT=Gruental, GK=Gardner&Knopoff (1974), UH=Uhrhammer (1986)).

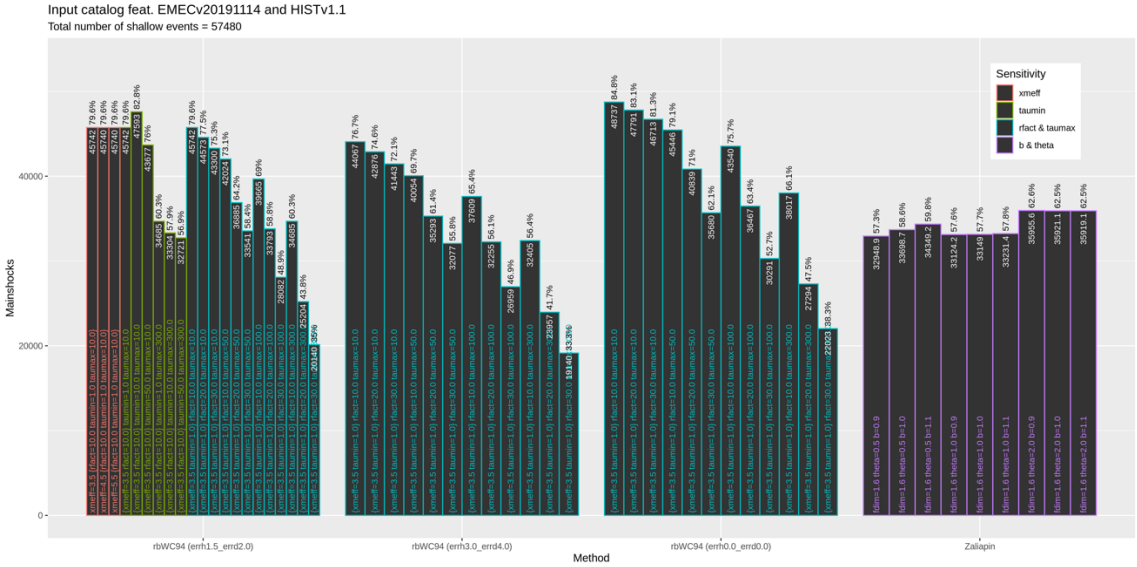

Figure 4: Parameter sensitivity overview for all conducted cluster-based and stochastic declustering methods (rb=Reasenberg(1985), Zaliapin=Zaliapin et al. (2008).

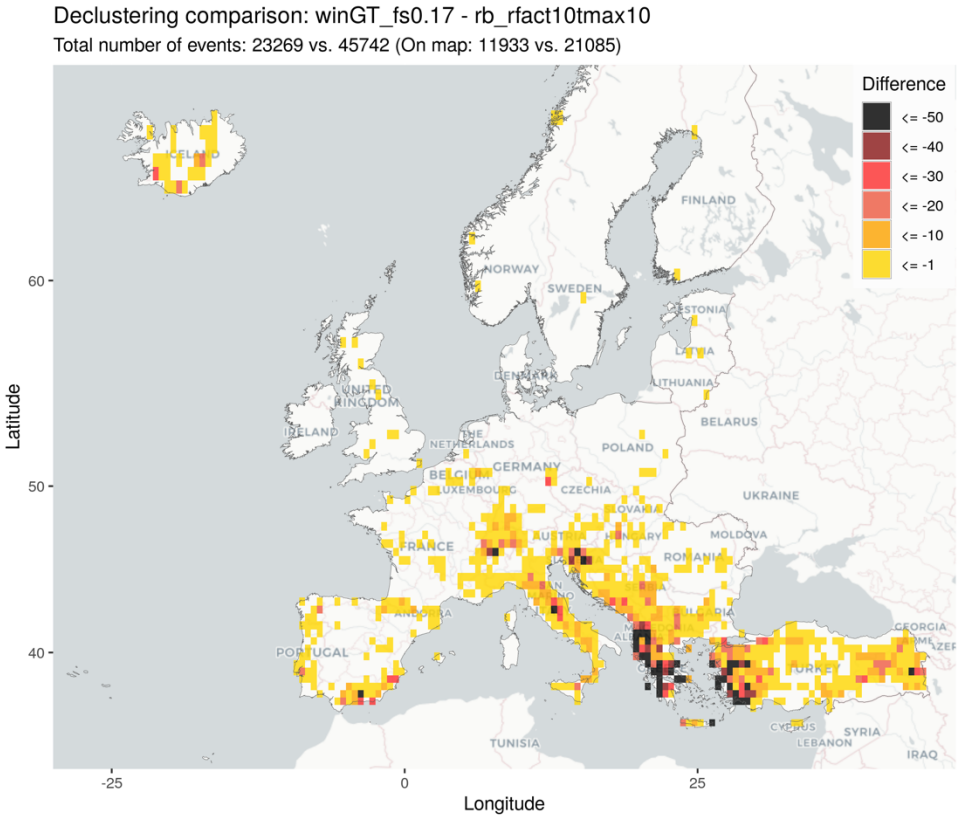

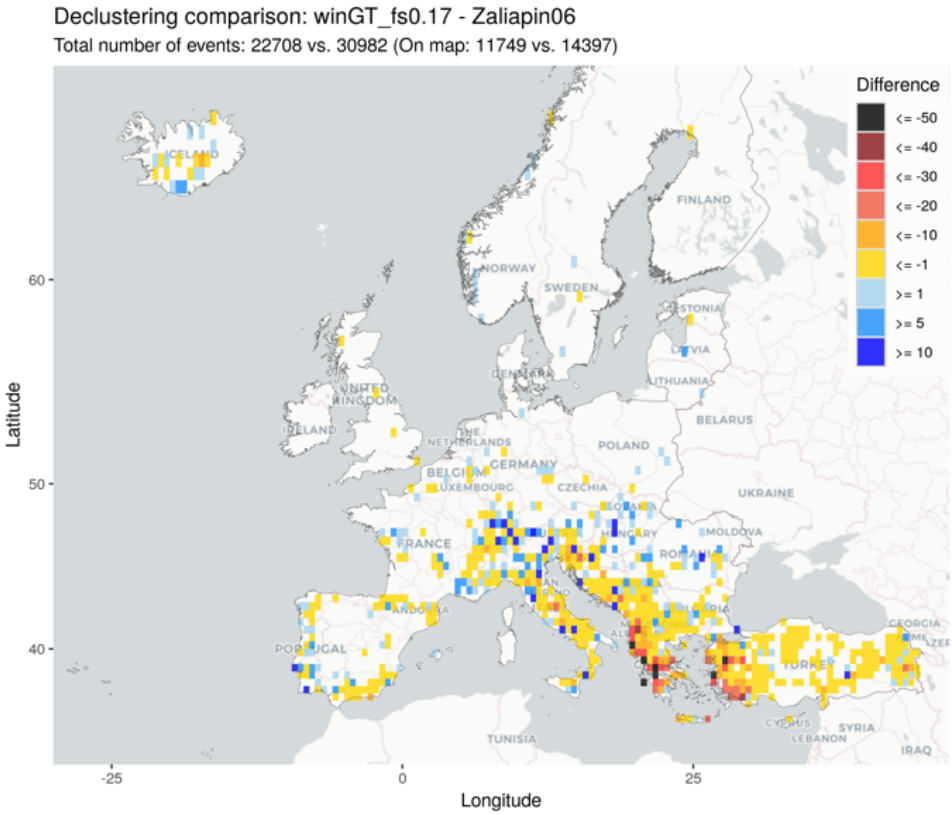

Figure 5: Spatial difference of the number of events with magnitude M >4.5 in a 50km grid cell, comparing the time-window based method (GT=Grünthal ESHM13) with rb=Reasenberg (1985) (top), and with Zaliapin=Zaliapin et al. (2008) (bottom).

2.1.2 Declustering Techniques: Statistical Evaluation

We performed Kolmogorov–Smirnov (KS) tests on the time distribution of all resulting mainshock catalogs and found that all of those techniques lead to declustered catalogs that obey a stationary Poisson distribution in most tectonic regions, thus we could not discriminate between declustering methods based on such an analysis.

Instead, we propose to use Collaborative for Study of Earthquake Predictability (CSEP, http://cseptesting.org/) comparison likelihood tests to evaluate the performance of declustering (by using the same method for earthquake activity rate estimation and varying the input catalog according to the declustering method). The key components of the procedure are:

- Learning catalogue: we convert all declustered catalogues into activity rate forecasts using earthquake catalogue data only till 12/2006 (learning catalogue). Activity rates were estimated for each completeness super zone given the corresponding completeness time history. We used the method of Weichert (1980) to compute a- and bGR-values in each super zone.
- Target catalogue: We use all events above moment magnitude Mw 4.5 from 1/2007 to 12/2014 as target events. This target catalogue contains 2107 events.
- Likelihood comparison tests: CSEP's comparison likelihood tests address the question which of two models is better, i.e. which model shows a higher forecasting skill in comparison to the other. Rhoades et al. (2011) introduced two suitable statistical tests that

are based on estimates of the average-rate corrected information gain per earthquake (e.g. Harte and Vere-Jones, 2005; Imoto and Hurukawa, 2006).

The procedure is described in details in the SERA D25.3 deliverable and not repeated here. We compared two activity rate forecasts using the target catalogue on the basis of their forecasted spatial distribution. To isolate the spatial information from a forecast, one computes the sum of all magnitude bins, and the resulting forecast sum is normalized so that it matches the observed number of target events.

We use the windowing declustering method of Grünthal (1985) as our reference forecasts (vertical black lines in Figure 6). We chose this method as our reference because it was used as the principal declustering technique in ESHM13. Considering the large number of target events, we applied the T-Test to evaluate the significance of the likelihood differences as a function of space between the reference model and all other selected declustering techniques.

We find that all selected alternative declustering techniques have a positive information gain over the reference method (apart from Reasenberg using extreme end-member parameters), and that the likelihood gains are significant (red * in Figure 6).

Recommendation for model development: In the spatial domain, our findings support the use of the Reasenberg declustering method. Overall, our results suggest that Reasenberg algorithm should be considered as a valid alternative to the window-based reference method.

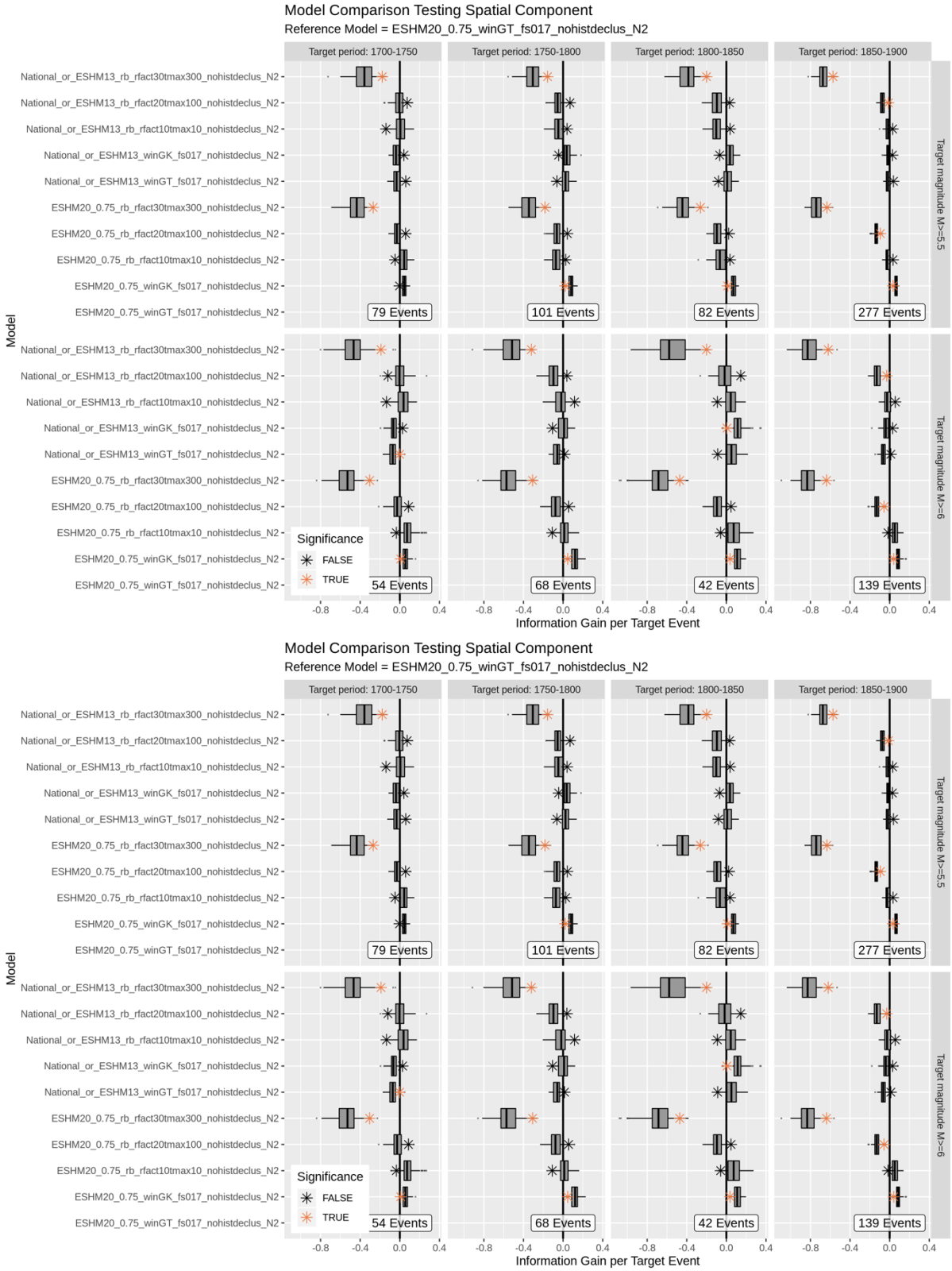

Model Comparison Testing Spatial Component
Reference Model = ESHM20_0.75_winGT_fs017_nohistdeclus_N2
Target period: 1700-1750
Target period: 1750-1800
Target period: 1800-1850
Target period: 1850-1900
Target magnitude M>=5.5
Target magnitude M>=6
Model
National_or_ESHM13_rb_rfact30tmax300_nohistdeclus_N2
National_or_ESHM13_rb_rfact20tmax100_nohistdeclus_N2
National_or_ESHM13_rb_rfact10tmax10_nohistdeclus_N2
National_or_ESHM13_winGK_fs017_nohistdeclus_N2
National_or_ESHM13_winGT_fs017_nohistdeclus_N2
ESHM20_0.75_rb_rfact30tmax300_nohistdeclus_N2
ESHM20_0.75_rb_rfact20tmax100_nohistdeclus_N2
ESHM20_0.75_rb_rfact10tmax10_nohistdeclus_N2
ESHM20_0.75_winGK_fs017_nohistdeclus_N2
ESHM20_0.75_winGT_fs017_nohistdeclus_N2
79 Events
101 Events
82 Events
277 Events
54 Events
68 Events
42 Events
139 Events
Significance
FALSE
TRUE
-0.8
-0.4
0.0
0.4
Information Gain per Target Event

Figure 6: Information gain per event as a function of declustering method for various completeness solutions: ESHM20, ESHM13 and/or National.

2.1.3 Sensitivity Analysis of the Completeness Analysis

Size of magnitude bins for statistical estimates of seismicity parameters (a, b values)

First sensitivity analysis of the completeness analysis is the impact of the magnitude bin size in estimating the activity parameters: a- and b-values. In Figure 7(a), we show the empirical magnitude frequency distributions (EMDs) for the shallow earthquake catalogue for the three choices of magnitude bin sizes (Δm). To obtain these EMDs, we first discretize the magnitudes reported in the shallow earthquake catalogue using either $\Delta m = 0.1, 0.2,$ or 0.3. We then count the number of times the different discrete magnitudes appear in the discretized catalogue.

Recommendation for model development: The results indicate that an appropriate bin size for the catalogue might be $\Delta m = 0.1$ or $\Delta m = 0.3$ as the a-value and b-value are identical.

Sensitivity to magnitude completeness for statistical estimates of seismicity parameters (a, b values)

Figures 7(b) and 7(c) illustrate the dependence of the estimates the b and a values on the choice of the magnitude of completeness (M_c) for the three $\Delta m's$.

The estimates of b values are obtained using the following formula, which is valid for the magnitudes discretized at Δm intervals [Tinti and Mulargia, 1987; Marzocchi and Sandri, 2009].

$$b = \ln\left(1 + \frac{\Delta m \times N}{\sum_{i=1}^{N}(m_i - M_c)}\right) \times \frac{1}{\Delta m} \times \frac{1}{\ln 10} \qquad (1)$$

In Equation 1, the m_i's are N discrete magnitudes ($\geq M_c$) reported in the catalog.

Having estimated the b values, the a values can be estimated using the following formula:

$$a = \log_{10} N - \log_{10}\left(\sum_{j=1}^{K} 10^{-b\left(m_j - \frac{\Delta m}{2}\right)}\right) - \log_{10}\left(1 - 10^{-b\Delta m}\right) \qquad (2)$$

Note that, the a-values reported in Figure 2 have to be normalized by the duration of the earthquake catalogue to obtain the usually reported 'yearly' a-values.

It is evident from Figure 7b and 7c that the choice of M_c has a major impact on the estimated of both b and a values, thus justifying the need for its proper assessment. We find that as we increase the value of assumed M_c, the estimates of b and a increase. However, at $M_c \approx 4.8$, the estimates of both these parameters attain stability and do not change significantly. We use the stability in the estimates of b and a values as a proxy for the completeness of the catalog [Cao and Gao, 2002].

Recommendation for model development: based on this analysis, we can consider the shallow ESHM20 catalogue to be complete for $M \geq 4.8$. A similar analysis for the catalogues of the deep earthquakes leads to the same outcome for the magnitude of completeness (Figure 8). We also find that the estimates of overall M_c are insensitive to the choice of Δm.

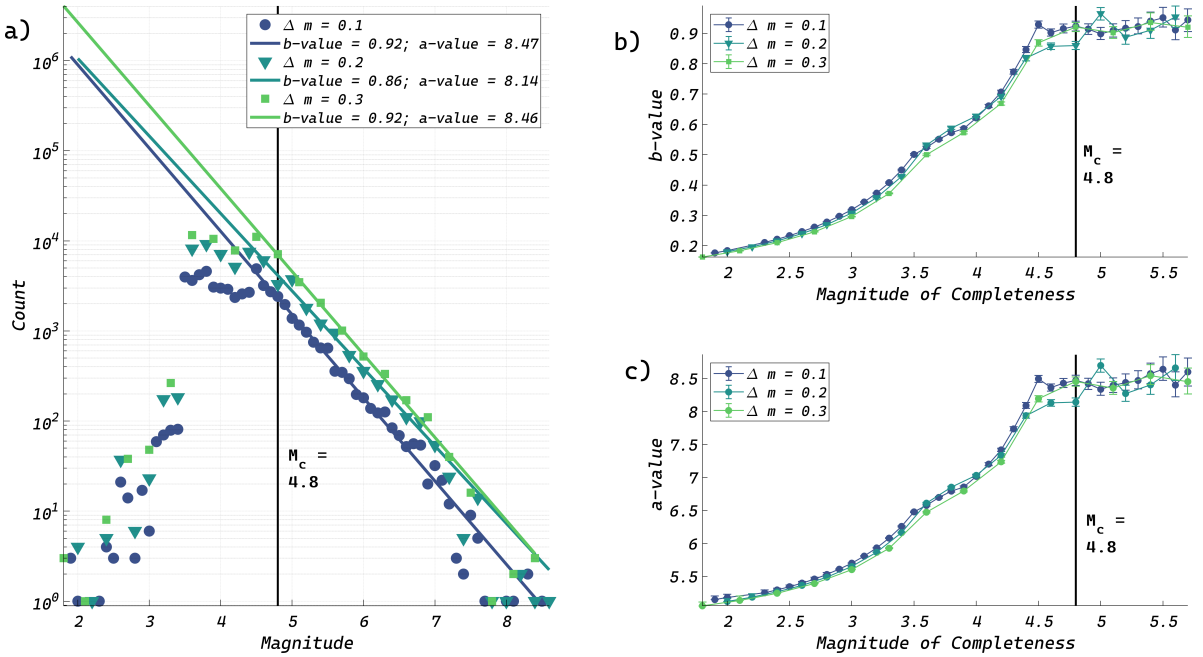

Figure 7: (a) Overall empirical magnitude distribution of the shallow earthquake catalog using three different magnitude discretization ($\Delta m = 0.1, 0.2\ and\ 0.3$); the estimated b-value and a-value, assuming $M_c = 4.8$, for the three different $\Delta m's$ are reported in the legend; (b-c) the estimates of b-value and a-value and their 95% confidence interval as a function of varying choice of M_c for the three different $\Delta m's$; both b-value and a-value seem to stabilize for $M_c \approx 4.8$, thus justifying the decision of choosing $M_c = 4.8$ as the global estimate.

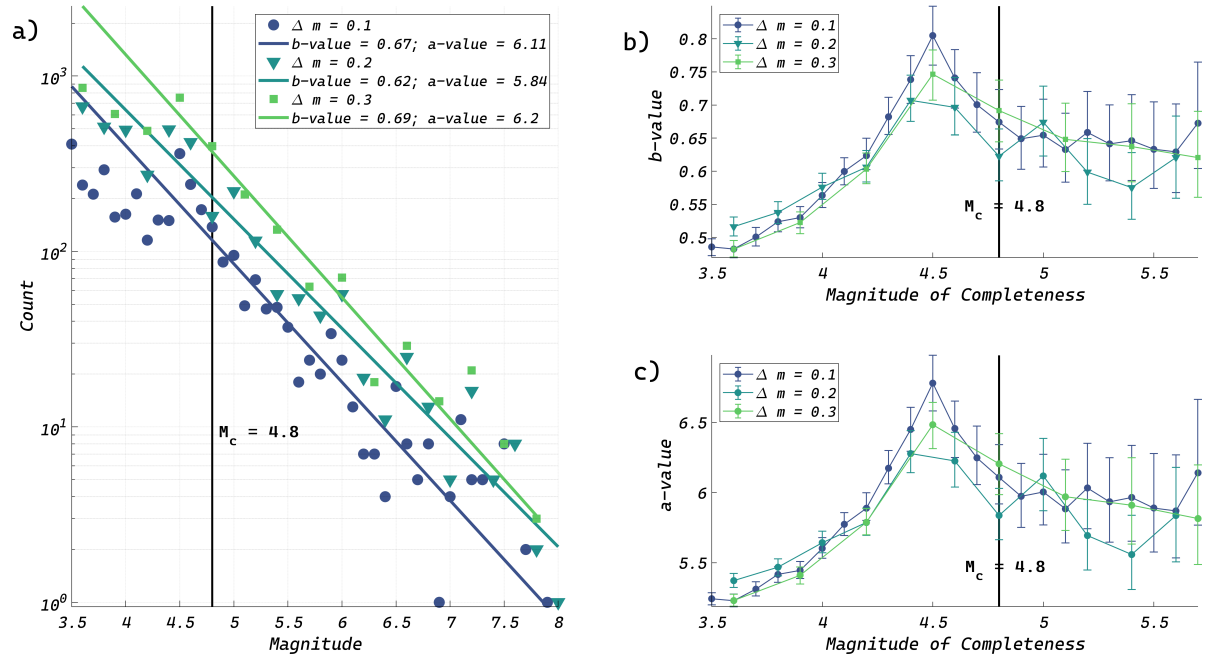

Figure 8: Same as Figure 7 but for the catalogue of the deep earthquakes (depth >60km)

2.1.4 Sensitivity Analysis of the Joint Declustering and Completeness Analysis

A newly developed technique to estimate the magnitude of completeness was developed within the SERA JRA2 and JRA3 coordinated efforts. The technique is data driven and aims at decupling the subjective judgment of experts.

The method is summarized in the SERA D25.3 - update M6 and not repeated herein. The proposed algorithm assumes that the magnitude of completeness (M_c) is piecewise constant within each of the time periods and it can be estimate by a non-parametric Maximum-Curvature method. The method was applied to completeness super-zones (we refer to 1.2 of SERA D25.3 update M36) and using various declustering algorithms. Thus, a sensitivity analyse was conducted to investigate the effect of the various declustering algorithms and the magnitude of completeness time series (MCTS) for every region.

Figure 9 illustrates the impact of the declustering method on the magnitude of completeness time series (plotted as red step curves on the right panel). The blue line in the same plot indicate the completeness of the ESHM13 model (based on expert opinions). The left panels indicate the magnitude frequency distributions obtained by applying the windowing declustering method of Grünthal (1985) and the Reasenberg technique (1985). Note that the declustering catalogue is a precondition of the data driven completeness method used for ESHM20. As expected the magnitude of completeness are slightly different for different declustering techniques, as also seen in a source in Turkey in Figure 10; the completeness Mc- time intervals are different (the red stair curves) as well as the magnitude frequency distributions given in left panel of the same plot. It is worth mentioning that we have conducted the sensitivity analysis for all declustering techniques investigated in the previous section and the completeness was re-evaluated.

Recommendation for model development: The results of the sensitivity analysis indicate that the magnitude of completeness time series (MCTS are robust for either windowing declustering method of Grünthal (1985) or the Reasenberg technique (1985). Thus, it is recommended to be either considering both in a logic tree framework. At this point for optimization of the calculation the windowing declustering method of Grünthal (1985) was used as the default method for estimating the magnitude of completeness in ESHM20.

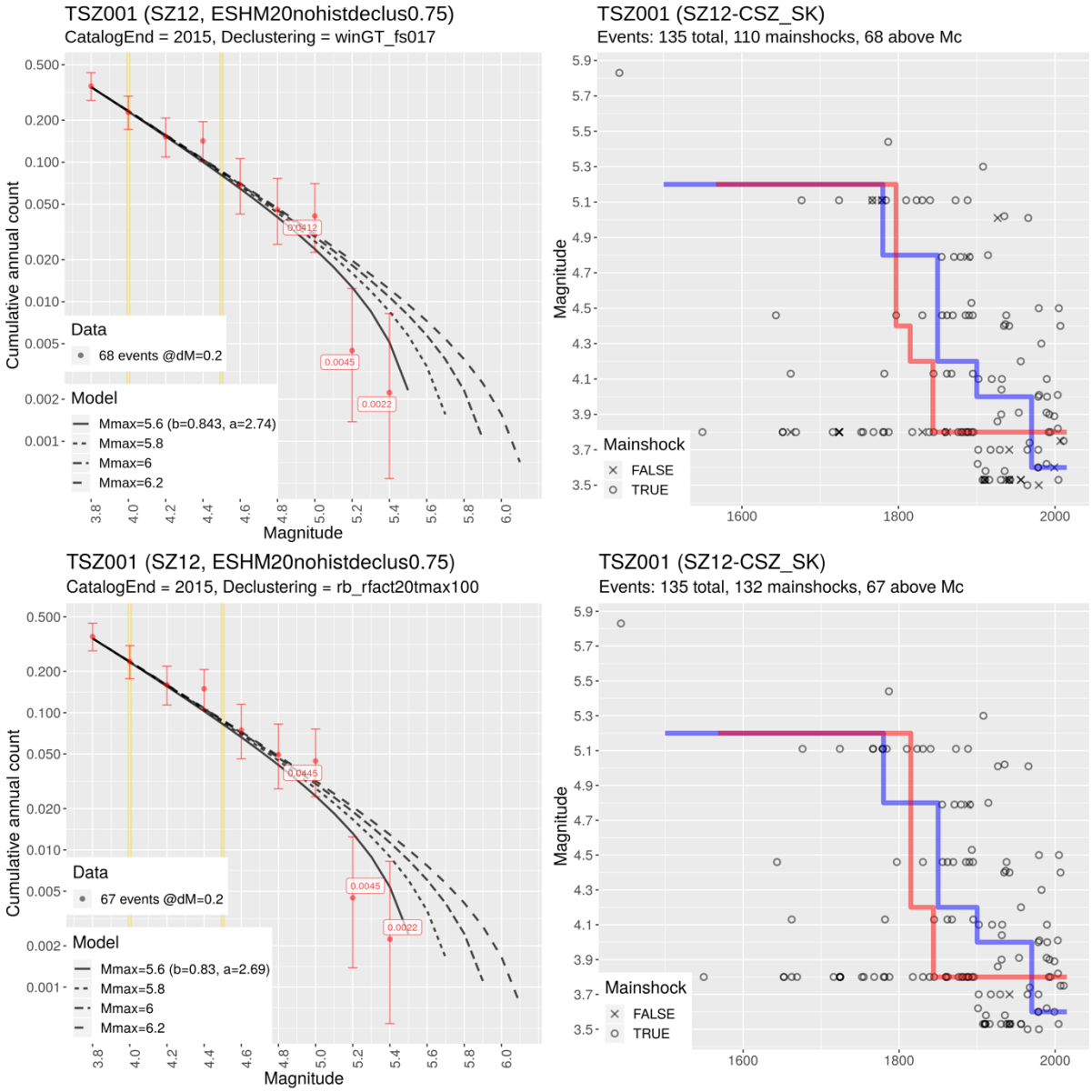

Figure 9: Sensitivity to the declustering algorithm used to automatically estimate the Mc-Time intervals plotted as step curves in the right panel. The top plots are for the windowing declustering method of Grünthal (1985) and bottom ones of Reasenberg technique (1985). The magnitude frequency distributions are displayed on the left panels. Note, the slight differences in a-, b-values and number of events above completeness. The blue step line in the right panels describe the ESHM13 completeness magnitude-time intervals. This example is for a source in Czech Republic.

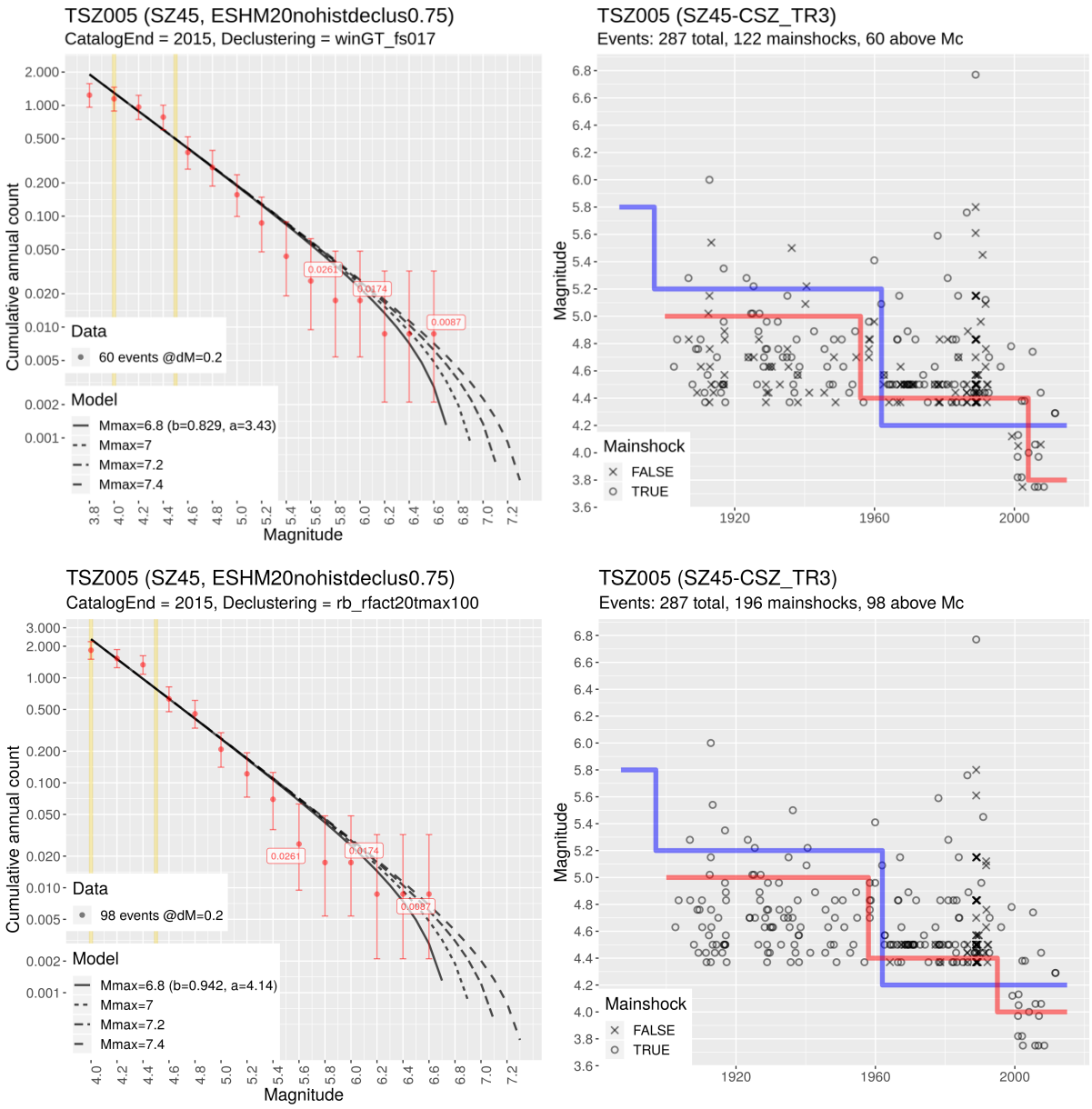

Figure 10: Same as Figure 9 but the example is for source in Turkey.

2.1.5 Comparison of the ESHM20 completeness vs National or the ESHM13 or completeness

An important comparison and sensitivity analysis are the investigation of the completeness and declustering analysis in comparison with the ESHM13 model.

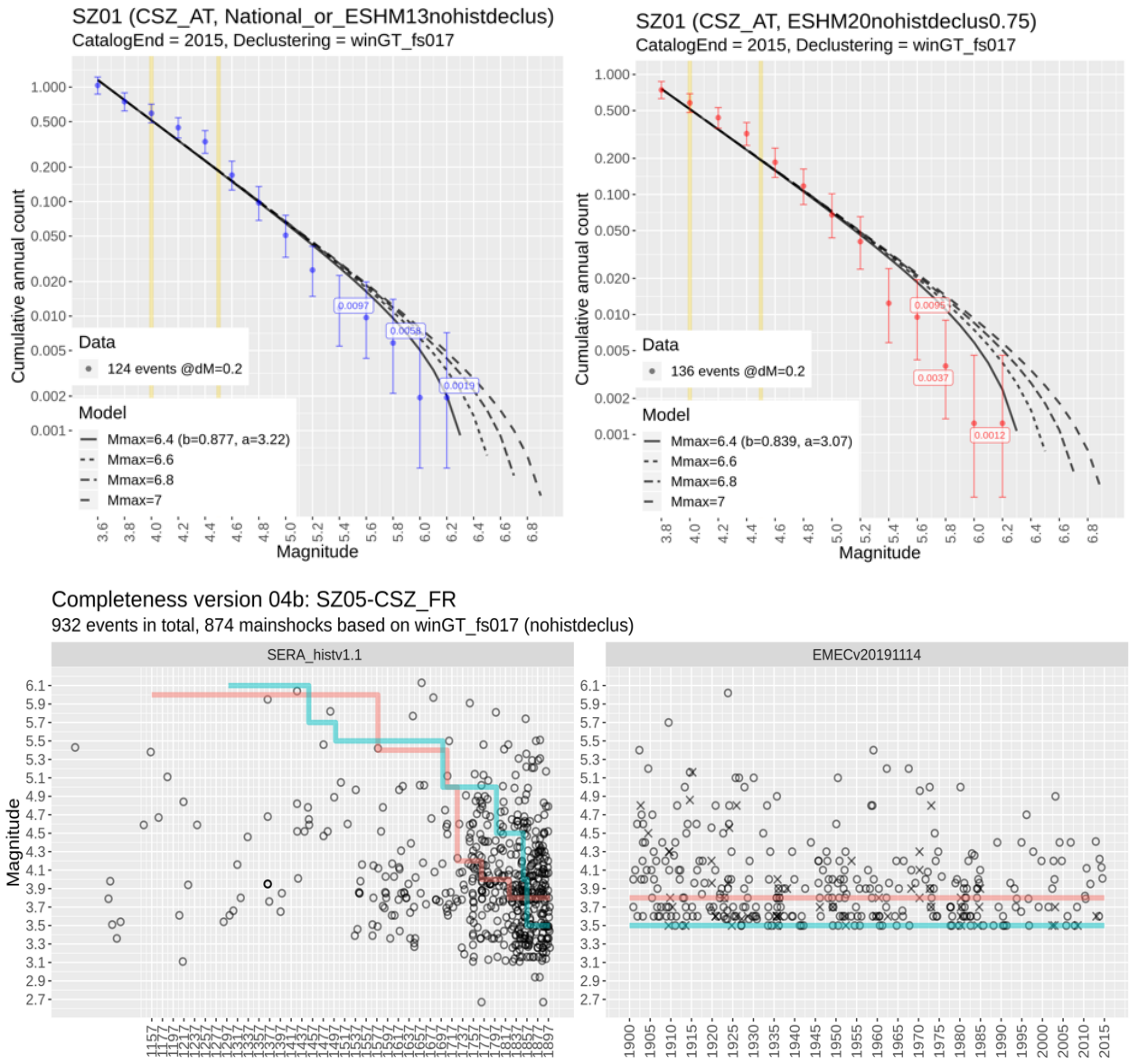

Figure 11: Effect of the ESHM13 vs ESHM20 completeness intervals for a super-zone in France. The upper plots indicate the magnitude frequency distribution of the two considered completeness estimates.

The comparison was conducted for the entire Europe and the results are illustrated in Figure 10, where the two-joint combination of declustering algorithms and their resulting completeness Mc-time intervals are compared. We keep as reference the windowing declustering method of Grünthal (i.e. GT_fs_017 in the plot) and compare with the outcomes of the Reasenberg declustering technique. The maps on the left-hand side indicate the total number of events in the catalogue, by using the two different completeness options: ESHM20 or the national completeness Mc-time intervals. Here, we refer to the national (as the latest study on the topic reported for that region). If there was no update at the national level, the ESHM13 completeness information was retained. It can be observed that the overall number of events is rather consistent between the ESHM20/ESHM13 completeness, but the differences are on specific region, where the differences in number of events are obvious (difference maps on the right-hand side on each figure). These results suggest that the national hazard models are

a viable alternative to the ESHM20, and this matter should be further investigated. However, at the time of the deliverable, this option was not yet considered.

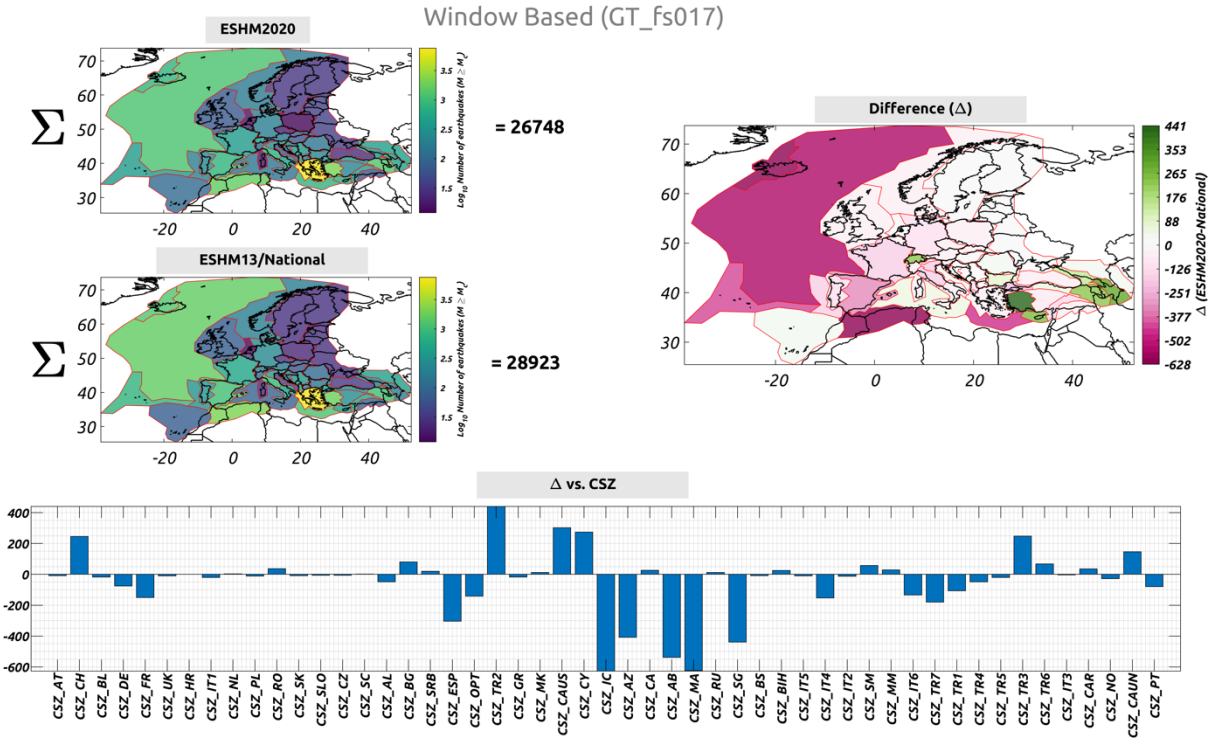

Figure 12: Comparison of the number of events per super-zones (CSZs) after applying the joint declustering and completeness Mc-time intervals of ESHM20 vs the National/ESHM13 completeness. The plots are valid for the reference declustering method of Grunthal (1985)

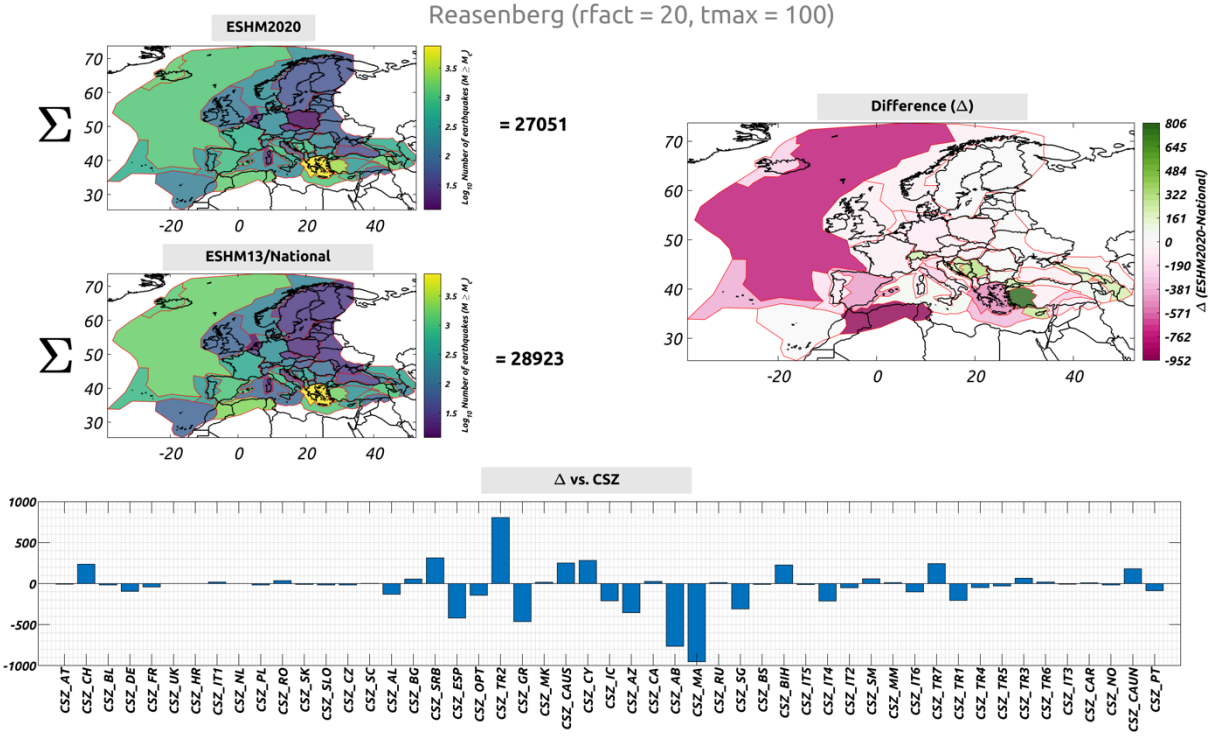

Figure 13: Comparison of the number of events per super-zones (CSZs) after applying the joint declustering and completeness Mc-time intervals of ESHM20 vs the National/ESHM13 completeness. The plots are valid for the reference declustering method of Reasenberg (1985)

2.2 Seismogenic Sources: Sensitivity Analysis

The main sensitivity analyses conducted on the seismogenic sources can be summarized as:

– Active Faults Characterization: impact of the key input parameters to total seismic productivity: fault area, slip-rates and maximum magnitude.

– Subduction interface characterization: impact of the key input parameters to total seismic productivity: fault area, slip-rates and maximum magnitude.

– Spatial variability of the Maximum Magnitude

2.1.6 Active Faults: sensitivity on the key input parameters: fault area, slip-rates and maximum magnitude

To characterize the seismic activity of active faults, the long-term geological slip rates are used. The geological slip-rates describe several seismic cycles of large-magnitude earthquakes on a fault offering advantages over historical seismicity when used to estimate the earthquake frequency. In ESHM13, we used the Model 2 of Anderson and Luco (1983) and herein after we the effect of key input parameters to the fault seismic productivity.

For all cases, the following values were considered as default: crust shear modulus (μ) value of 3.0 x 1e11 dyne/cm2; typical values (c=16.05 and d=1.50) for the magnitude-moment scaling coefficients as originally proposed by Kanamori and Anderson (1975); an average value of fault-slip to fault length ratio (α =1.25 x 10-5) as originally recommended by Anderson and Luco (1983).

Figure 12 illustrates the effects of the key input parameters on the magnitude frequency distributions of a single fault. The effect of the slip-rates variability of a single fault with a constant b-value, fault area and maximum magnitude Mw=7.0 is given in Figure 14a. As expected the highest the slip-rate the highest the total seismic productivity of a single fault. Figure 14b illustrates the sensitivity of seismic productivity of the fault given different reported values for the fault area, as indicated in the database of the active faults. It can be observed that the area has a significant impact to the total productivity, the large the area of the fault the higher the seismic productivity. However, the fault area is correlated with the maximum magnitude of the faults, thus it requires a-priori check of the consistency between these two parameters.

Third sensitivity case study investigates the effect of maximum magnitude. For a constant slip rate, increasing the Mmax will result in decrease in the recurrence rates of low-to-moderate magnitude events. This is because the large magnitude events will quantify the majority of the total seismic moment rate, while increasing the magnitude will require a subtraction of many smaller earthquakes to preserve the same seismic moment budget (Youngs and Coppersmith 1985). This is obvious in the Figure 14c. The last sensitivity analysis illustrates the effect of the b-value variability, which is again obvious from the plot that the high b-values will tend to increase the forecast of low magnitude bins, and when coupled with the conservation of the seismic moment budget, the effect can be significant (Figure 14d).

Recommendation for model development: The sensitivity analysis indicates that the key parameters play significant role on the total seismic productivity of the fault. To capture the epistemic uncertainties the following key parameters are proposed: three values of the slip-rates, three values for the maximum

magnitude, a single b-value (estimated from robust statistics in the TECTO zones) and an average area of the faults.

Thus, 9 combinations of seismic activity rates are considered to characterize the uncertainties of the seismic productivity of all active faults, two examples of two faults in Albania and Spain are given in Figure 15. Note, that the hazard integration starts at a minimum magnitude of 4.5Mw, thus the forecasted earthquake rates on the faults within the minimum magnitude and Mmax values is considered.

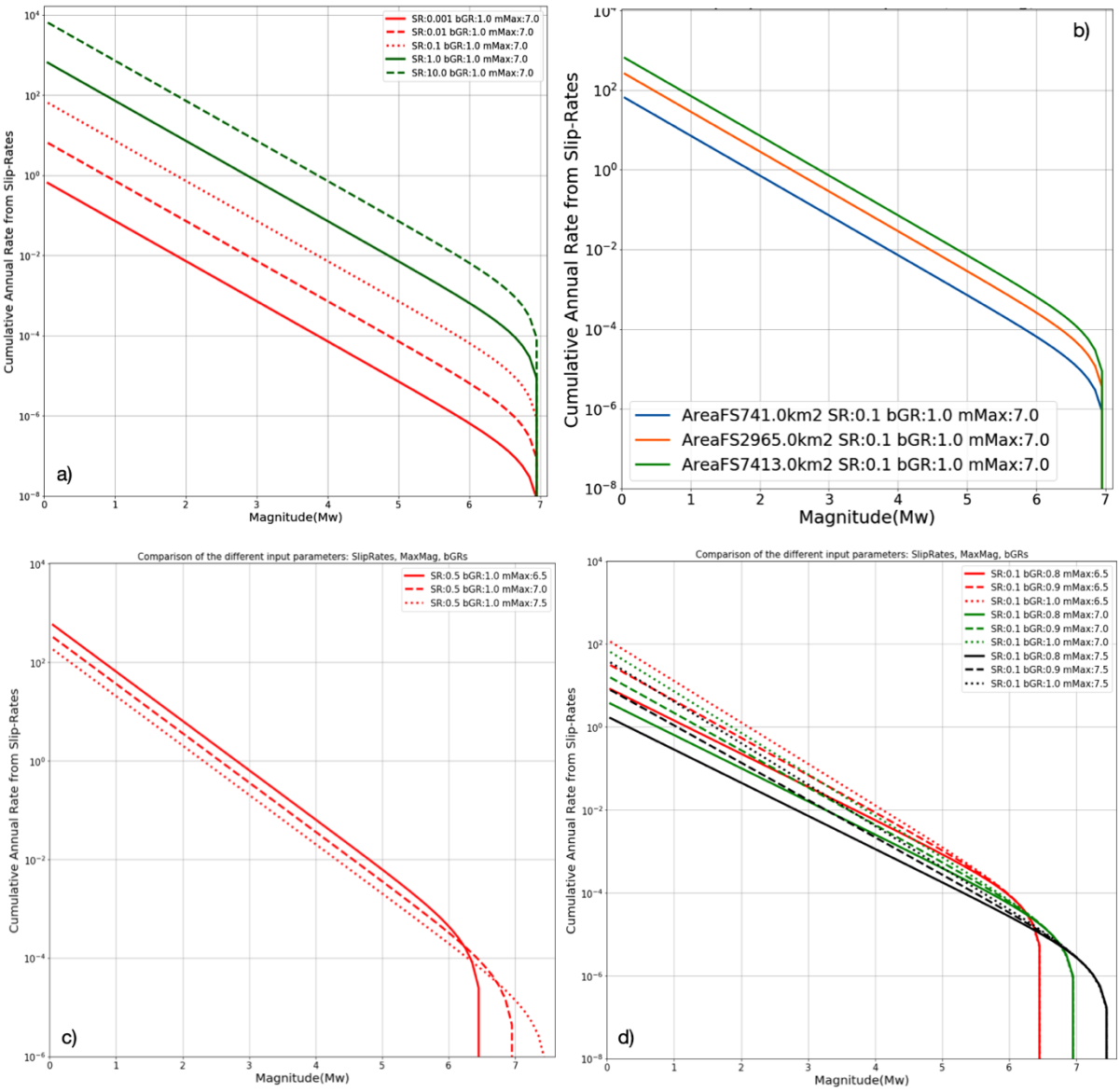

Figure 14: Effects of various key input parameters in seismic productivity of a single fault: a) variable slip-rates; b) variable fault area (in square-km); c) maximum magnitude d) variable b-values

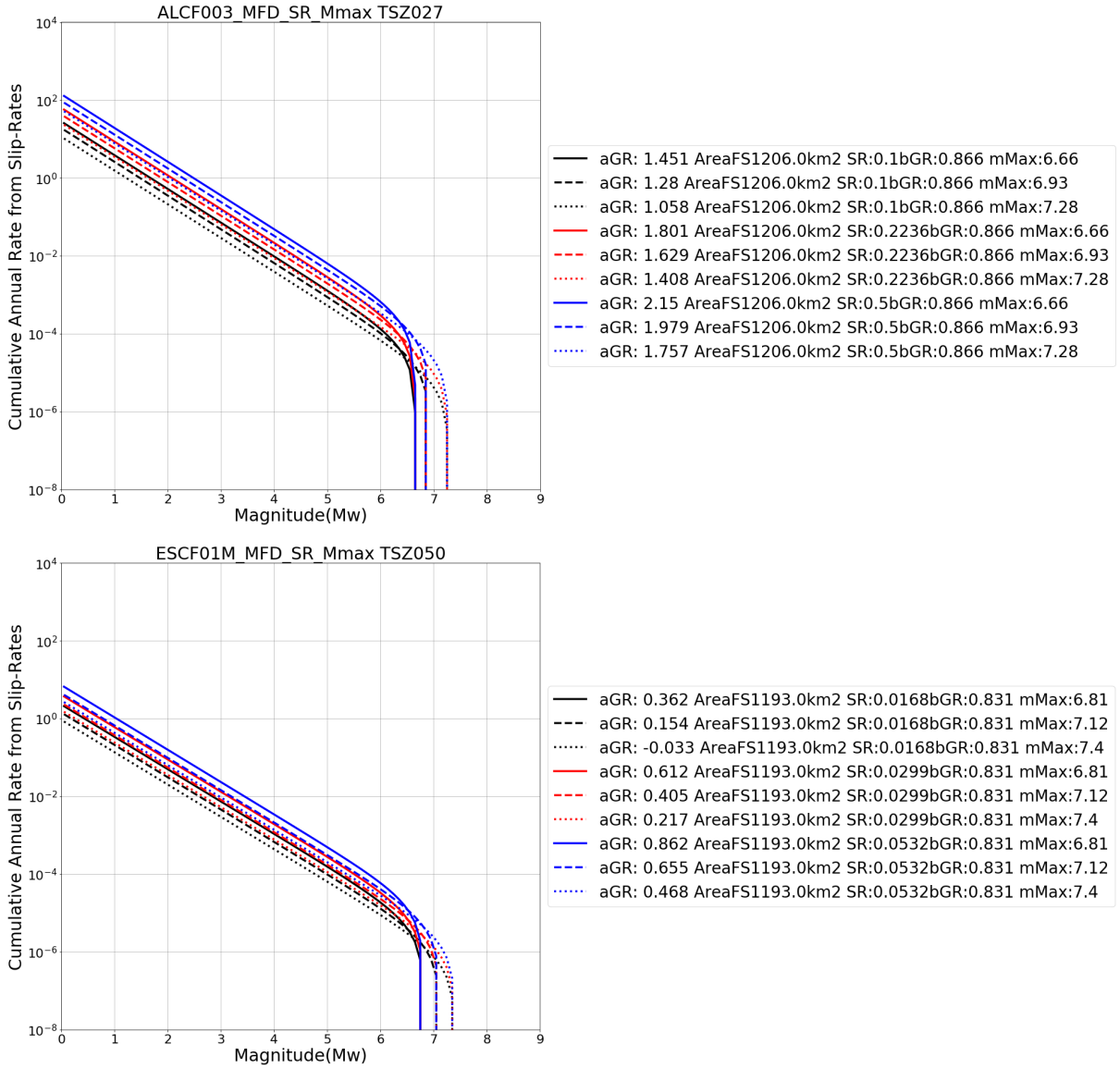

Figure 15: Magnitude frequency distributions of a single fault in Albania (top) and Spain (bottom) as resulting from combining variable slip-rates and maximum magnitudes. The regional b-value and the area of the fault are constant.

2.1.7 Subduction interface characterization: impact of the key input parameters to total seismic productivity: fault area, slip-rates and maximum magnitude.

The subduction model incorporates two different types of seismicity, in-slab and slab interface. The earthquake activity rates for these two types can be estimated from the unified earthquake catalogue. However, for the slab interface there is the opportunity to estimate the earthquake activity rates from the tectonic rates of convergence between the two plates across the subduction zone. This approach allows us to better capture the epistemic uncertainty of the long-term earthquake generation process in this critical tectonic environment.

The recurrence model is a double-truncated frequency-magnitude distribution that balances the seismic moment rate (Kagan, 2002). To estimate the activity rates, we set up a logic tree (Figure 16) that explores the contributions of a series of variables: upper and lower seismogenic depths, magnitude upper bounds, depth-dependent rigidity, tectonic rates, seismic efficiency, and b values.

Among these parameters, the geometry of the slab interface, the upper and lower seismogenic depths, and the tectonic convergence rates come from direct observational information, with their uncertainty. All the other parameters are rather indirectly derived; they come either from empirical relationships (magnitude upper bound and rigidity linked to slab interface area and position) or from subjective choices, though based on experience (e.g. Christophersen et al., 2015; Davies et al., 2019). In the following we illustrate the impact of these indirectly derived parameters.

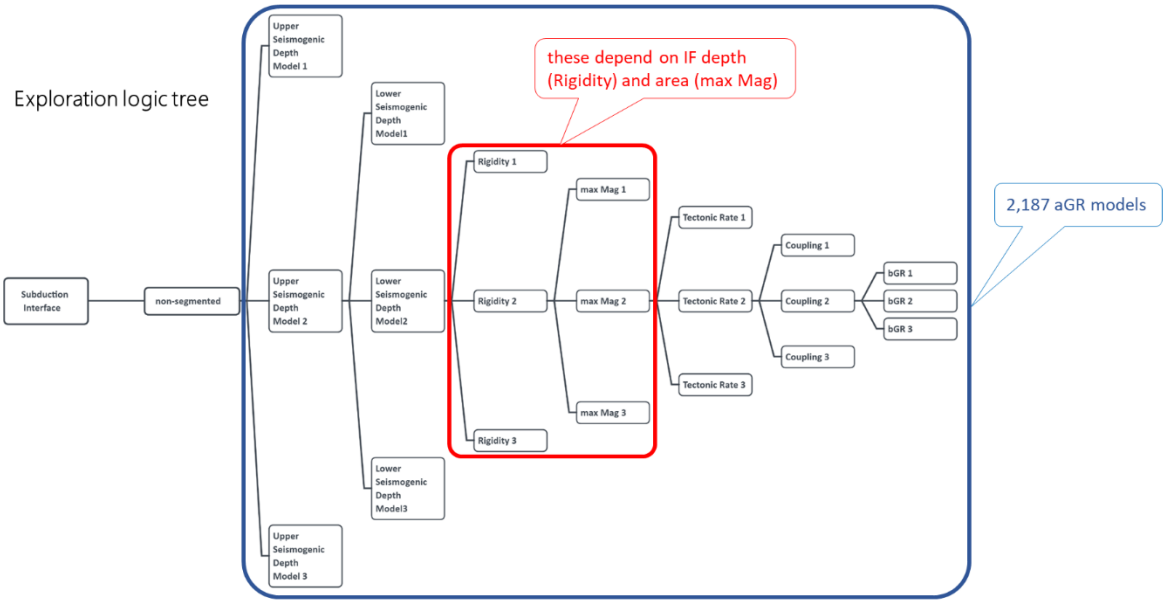

Figure 16: Logic tree designed to explore all the parameters that concur to estimate the earthquake activity rate to be converted into frequency-magnitude distributions.

The magnitude upper bound of the magnitude-frequency distribution is constrained by the scaling relations by Allen and Hayes (2017) and rigidity is constrained from the depth distribution by Sallarès and Ranero (2019). Figure 15 shows the distribution and variability of these two parameters as a function of area and depth range, respectively, as well as their comparison with other models available in the literature. The impact of seismic coupling and b value onto a double-truncated frequency-magnitude distribution is shown in Figure 17.

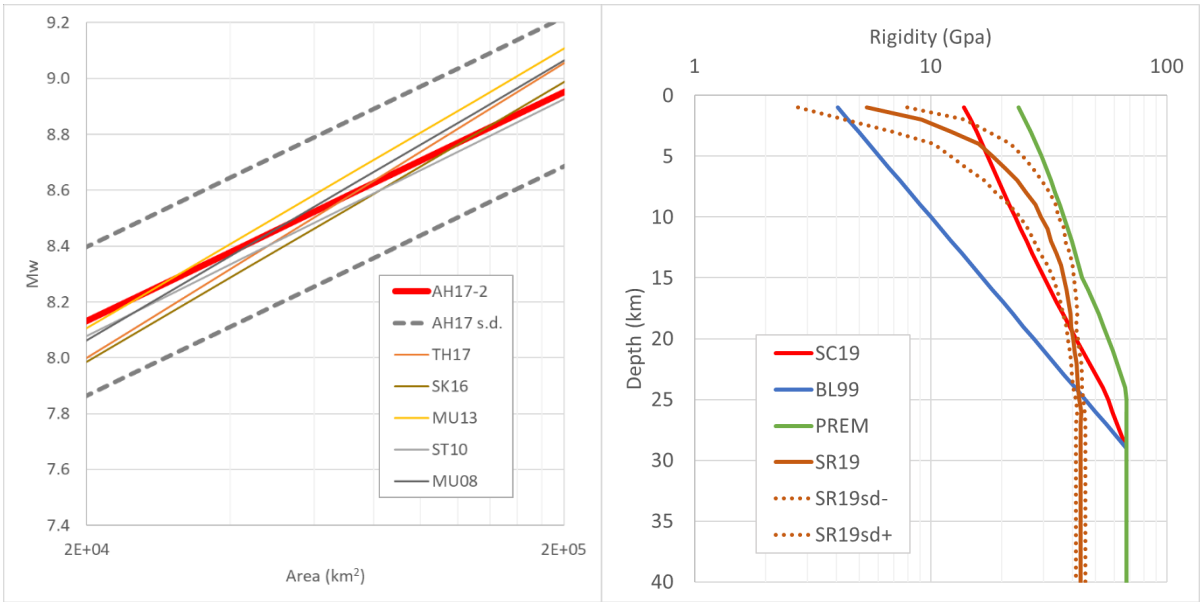

Figure 17: Comparison of rupture scaling relationships (left) in the range of rupture areas envisaged in the four slab interfaces of the hazard model: AH17 - Allen & Hayes, 2017, and its standard deviation; MU08 - Murotani et al., 2008; ST10 - Strasser et al., 2010; MU13 - Murotani et al., 2013; SK16 - Skarlatoudis et al., 2016; TH17 - Thingbaijam et al., 2017. Comparison of rigidity depth distributions (right) proposed or used in subduction zone models in the depth range the four slab interfaces of the hazard model: SC19 - Scala et al., 2019; BL99 - Bilek & Lay, 1999; PREM: Dziewonski & Anderson, 1981; SR19 - Sallarès and Ranero, 2019, and its standard deviation.

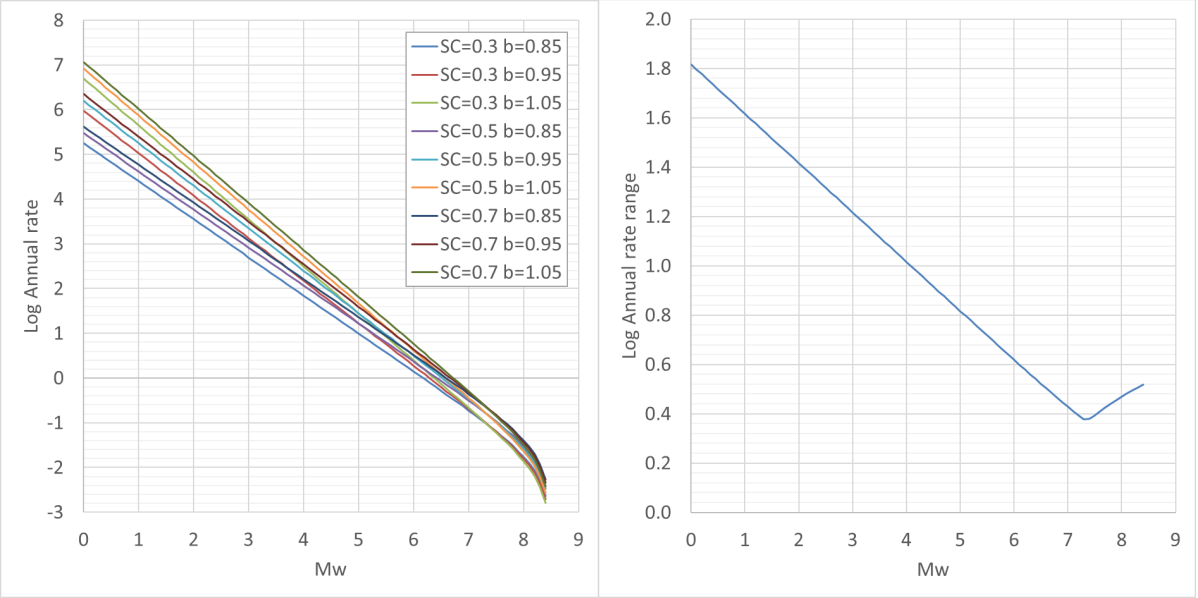

Figure 18: Comparison of moment-balanced frequency-magnitude distributions, following the formulation by Kagan (2002), depending on different b values and seismic coupling applied to a total moment rate of 3.3e+20 Nm/yr (left). Range of variability of the resulting earthquake annual rates.

The exploratory logic tree shown in Figure 16 with all these parameters yields 2187 different frequency-magnitude distributions. To reduce the computational cost implied by all these alternatives, we trimmed the exploratory logic tree by selecting three representative paths which excludes most of the branches that represents the extreme parameter alternatives. In this way we can narrow the alternatives down to three, preserving the exploration of almost the full range of earthquake annual rates in the magnitude range of interest for slab interface earthquakes. Figure 19 shows the percentile ranks of the three selected frequency-magnitude distributions compared with the distributions with the lowest and highest a value among the 2187 distributions resulting from the exploratory logic tree.

Note that the selected distributions approach the highest and lowest percentile rank as magnitude increases, in particular, when M is larger than 6.5. Note also that the intermediate model is slightly skewed upward at all magnitude values.

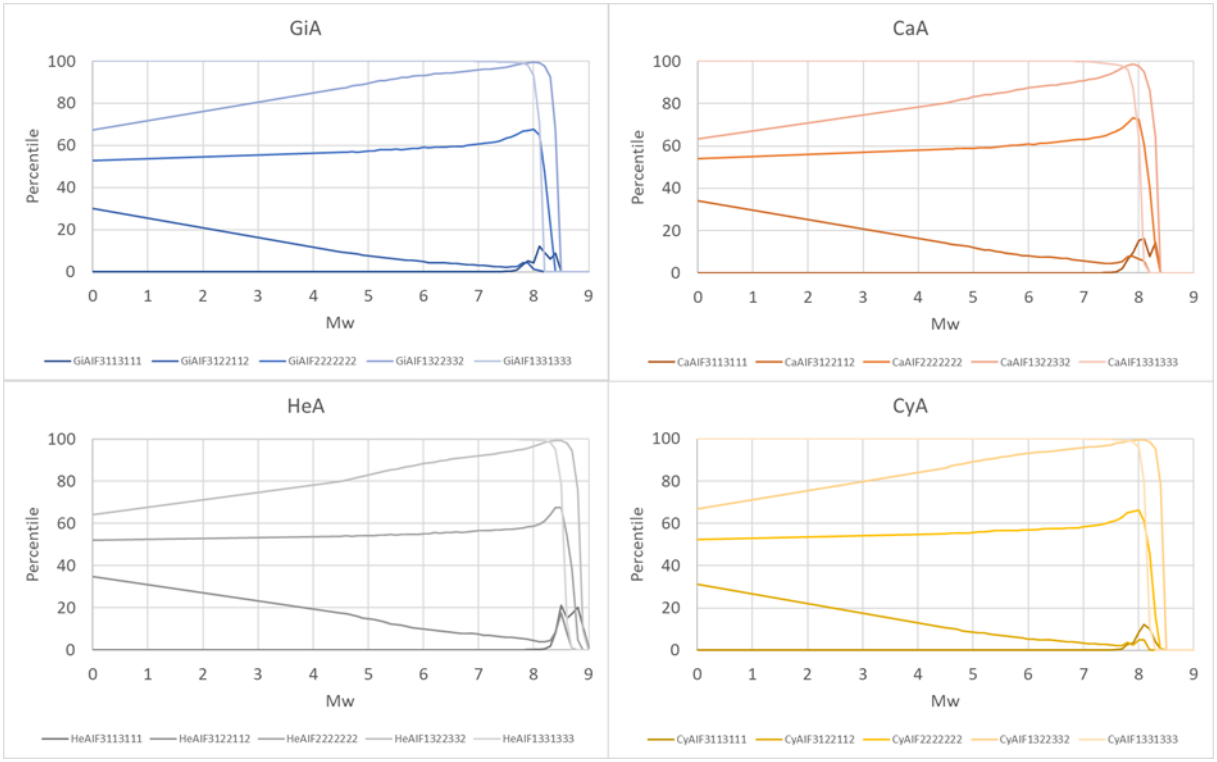

Figure 19: Percentile ranks of the frequency-magnitude distributions from the selected logic three branches for the four slab interface models: GiA - Gibraltar Arc, CaA - Calabrian Arc, HeA - Hellenic Arc, and CyA - Cyprus Arc. The darkest and lightest lines in each panel represent the distribution with the lowest and highest earthquake annual rates, respectively, of all the 2187 combinations of the exploratory logic tree.

2.1.8 Spatial Variability of the Maximum Magnitude

The maximum magnitude in the area source model of ESHM20 is based on the maximum magnitude values reported in ESHM13 (as summarized in the SHARE D3.3 Deliverable). In this section we investigate the range of maximum magnitude is the area source model versus maximum magnitude of obtained by the smoothed seismicity model (details in D25.3 updated M36). The maximum magnitude of the smoothed seismicity it corresponds to a maximum magnitude with an annual recurrence of 10-6, corresponding to a mean return period of 1mil years. Overall, in Figure 20 it can be observed that the values of the maximum magnitude of the area source model are more conservative than those corresponding to those values of the smoothed seismicity. This expected as the maximum magnitude on the area are estimated with a long term forecast basis, as it is based on a basis of seismicity, active faults and tectonic domains.

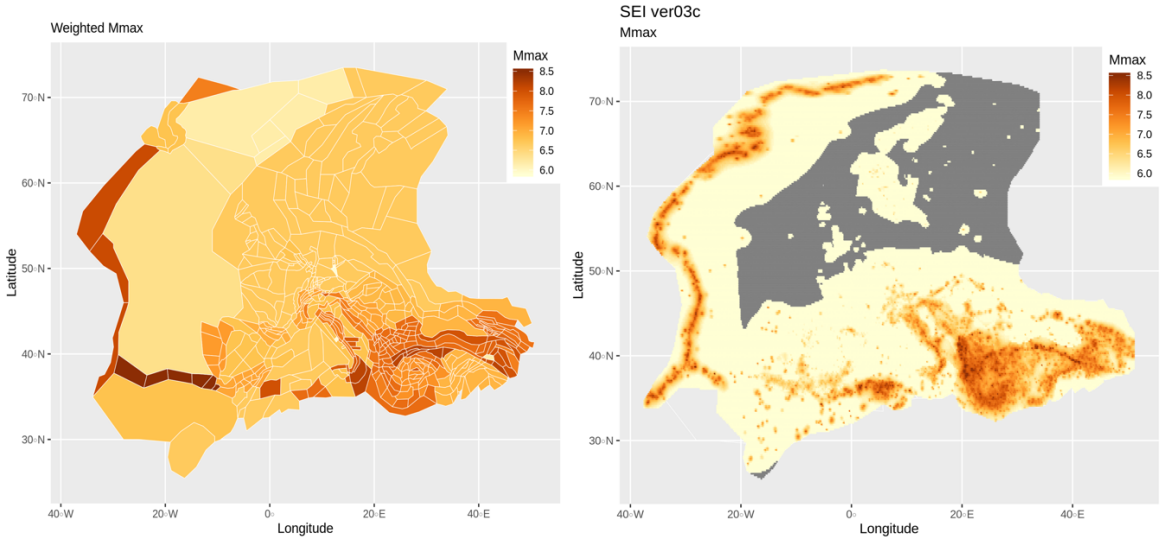

Figure 20: Spatial distribution of the maximum magnitude derived as retained from the area source model (left) and the maximum magnitude corresponding to an annual recurrence rate of 10e-6 of the smoothed seismicity model (see SERA Deliverable D25.3)

3 Hazard Calculation: Output

The hazard calculation will be tailored to match the engineering requirements listed in SERA JRA3 Deliverable - D25.1. The engineering community requirements are mainly defined by the needs of the ongoing revisions to Eurocode 8, whereas the risk modelling needs have been identified by participants of the SERA work-package JRA4 (Risk Modelling Framework for Europe). The computational grip point is illustrated in Figure 2. For more than 120 000 point it will be provided the weighted mean, median (50^{th}) and four quantiles (5^{th}, 16^{th}, 84^{th} and 95^{th}) for various intensity measure types: peak ground acceleration (PGA), peak ground velocity (PGV), and response spectra acceleration with 5% damping at predominant periods in the range of 0.05s to 8s. The reference site conditions are $V_{s,30} \geq 800$ m/s. The main results are:

1. Hazard maps for specified intensity measure types and five mean return periods (i.e. 50, 475, 975, 2500 and 5000 years)
2. Hazard curves at every computational site, depicting the mean, median (50^{th}) and four quantiles (5^{th}, 16^{th}, 84^{th} and 95^{th}) for all intensity measure types
3. Uniform Hazard Spectra at every computational site, depicting the mean, median (50^{th}) and four quantiles (5^{th}, 16^{th}, 84^{th} and 95^{th}) and five mean return periods (i.e. 50, 475, 975, 2500 and 5000 years)
4. Disaggregation of the hazard results for PGA and the two anchoring points of the EC8 design spectra (SA[0.05s] and SA[1.0s]). The disaggregation will be reported either as a controlling scenario of various intensity measure types for specified return periods (Figure 21) or as full 3d histograms.

Of a particular interest are the two main products to be produced as a basis for an update of the informative annex of Eurocode 8, Part 1). These two products, also summarized in SERA D25.7 are as follows: 1) European map of the median elastic spectral acceleration of the plateau[1]* of the response spectrum on reference rock with a Vs30 of 800 m/s. 2) European map of the median elastic spectral acceleration at 1 second on reference rock with a Vs30 of 800 m/s. The results as well as the main inputs of the ESHM20 will be online available and free to access throughout the web-platform of European Facilities of Earthquake Hazard and Risk (EFEHR) – www.efehr.org.

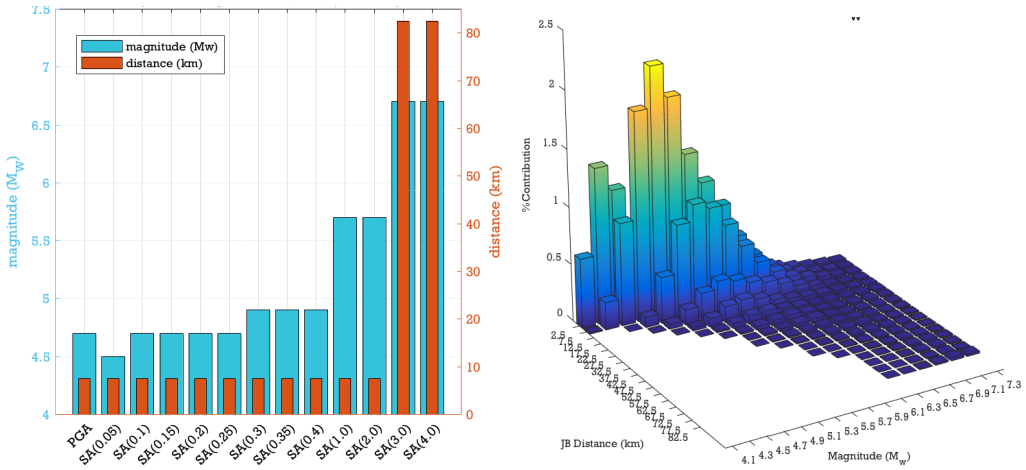

Figure 21 Example of the disaggregation output: controlling scenarios (magnitude and distance) for various intensity measure types (left) contribution matrix of magnitude and distance bins for PGA. The same type of output will be used to display the disaggregation of the ground motion hazard in ESHM20

[1] The definition of the plateau of the spectrum is being provided by a working group of CEN/TC250/SC8.

4 Hazard Calculation: Computational Infrastructure

2.1 Software Capabilities

OpenQuake is built on open-source and open-standard and freely available. The software is a collection of Python libraries is under continue development and improvements. At the time (April 2019) of this report the latest version is 3.6, and we highly recommend to address the following resources for updates and new software releases:

OQ-engine main website http://www.globalquakemodel.org/openquake/start/engine/

OQ-engine bug tracking system: https://launchpad.net/openquake

OQ-engine web repository: https://github.com/gem/oq-engine

All input and output files are in standardized NRML input file format.

2.1.9 Hardware Capabilities

To facilitate the calculation of the ESHM20, a high-performance cluster with OpenQuake (32 nodes / 64 CPUs / 500 cores / 1 TB RAM / has been set up in cooperation with CSCS (Swiss National Supercomputing Centre).

2.1.10 Computational Time: Stress Test

Given our expertise in running the seismic hazard computation in ESHM13 with OpenQuake, we were able to profile the hazard parameters critical for controlling the total computational time, and the hardware capability described above:

- Number of the computational grid-points
- Number of seismic source models
- Number of tectonic regions
- Number of GMPEs for each tectonic feature
- Size of the hypocentral depth distribution
- Area source discretization/sampling intervals
- Fault source mesh sampling intervals
- Size of the magnitude-frequency distribution (MFD)
- Size of the MFD sampling bin
- Type of seismic hazard output
- Number of intensity measure types
- Ground motion discretization levels
- Type of summary statistics: mean and quintiles

Furthermore, a stress test has been conducted using the ESHM13 input models, and the computational time was about *3 hours*. This is a great performance given that in 2012 the computation time of the ESHM13 was about *4 weeks including post-processing*. The computational performance is due to hardware upgrade and improvements of the algorithms and optimization of the OpenQuake hazard libraries. The performance of the hardware-software system will facilitate the computation of all hazard requirements specified on Deliverable D25.1, including hazard disaggregation at various location in Europe.

5 References

Allen, T. I., & Hayes, G. P. (2017). Alternative Rupture-Scaling Relationships for Subduction Interface and Other Offshore Environments. Bulletin of the Seismological Society of America, 107(3), 1240–1253. https://doi.org/10.1785/0120160255.

Blaser, L., Kruger, F., Ohrnberger, M., & Scherbaum, F. (2010). Scaling Relations of Earthquake Source Parameter Estimates with Special Focus on Subduction Environment. Bulletin of the Seismological Society of America, 100(6), 2914–2926. https://doi.org/10.1785/0120100111.

Murotani, S., Miyake, H., & Koketsu, K. (2008). Scaling of characterized slip models for plate-boundary earthquakes. Earth, Planets and Space, 60(9), 987–991. https://doi.org/10.1186/bf03352855.

Murotani, S., Satake, K., & Fujii, Y. (2013). Scaling relations of seismic moment, rupture area, average slip, and asperity size for M ~9 subduction-zone earthquakes. Geophysical Research Letters, 40(19), 5070–5074. https://doi.org/10.1002/grl.50976.

Skarlatoudis, A. A., Somerville, P. G., & Thio, H. K. (2016). Source-Scaling Relations of Interface Subduction Earthquakes for Strong Ground Motion and Tsunami Simulation. Bulletin of the Seismological Society of America, 106(4), 1652–1662. https://doi.org/10.1785/0120150320.

Strasser, F. O., Arango, M. C., & Bommer, J. J. (2010). Scaling of the Source Dimensions of Interface and Intraslab Subduction-zone Earthquakes with Moment Magnitude. Seismological Research Letters, 81(6), 941–950. https://doi.org/10.1785/gssrl.81.6.941.

Thingbaijam, K. K. S., Martin Mai, P., & Goda, K. (2017). New Empirical Earthquake Source-Scaling Laws. Bulletin of the Seismological Society of America, 107(5), 2225–2246. https://doi.org/10.1785/0120170017.

Kagan, Y. Y. (2002), Seismic moment distribution revisited: I. statistical results, Geophys. J. Int., 148, 520–541.

Sallarès, V., & Ranero, C. R. (2019). Upper-plate rigidity determines depth-varying rupture behaviour of megathrust earthquakes. Nature, 576(7785), 96–101. https://doi.org/10.1038/s41586-019-1784-0

Bilek, S. L., & Lay, T. (1999). Rigidity variations with depth along interplate megathrust faults in subduction zones. Nature, 400(6743), 443–446. https://doi.org/10.1038/22739.

Dziewonski, A. M., & Anderson, D. L. (1981). Preliminary reference Earth model. Physics of the Earth and Planetary Interiors, 25(4), 297–356. https://doi.org/10.1016/0031-9201(81)90046-7.

Scala, A., Lorito, S., Romano, F., Murphy, S., Selva, J., Basili, R., Babeyko, A., Herrero, A., Hoechner, A., Løvholt, F., Maesano, F. E., Perfetti, P., Tiberti, M. M., Tonini, R., Volpe, M., Davies, G., Festa, G., Power, W., Piatanesi, A., & Cirella, A. (2019). Effect of Shallow Slip Amplification Uncertainty on Probabilistic Tsunami Hazard Analysis in Subduction Zones: Use of Long-Term Balanced Stochastic Slip Models. Pure and Applied Geophysics, 177(3), 1497–1520. https://doi.org/10.1007/s00024-019-02260-x.

Christophersen, A., Berryman, K., Litchfield, N. (2015) The GEM Faulted Earth Project, Version 1.0,

April 2015, GEM Faulted Earth Project, doi: 10.13117/GEM.GEGD.TR2015.02.

Davies, G., Griffin, J., Løvholt, F., Glimsdal, S., Harbitz, C., Thio, H. K., et al. (2019). A global probabilistic tsunami hazard assessment from earthquake sources. Geological Society, London, Special Publications, 456(1), 219–244. https://doi.org/10.1144/sp456.5.

Monelli D, Pagani M, Weatherill G, Danciu L, Garcia J (2014) Modeling Distributed Seismicity for Probabilistic Seismic-Hazard Analysis: Implementation and Insights with the OpenQuake Engine. Bull Seismol Soc Am 104(4): 1636–1649. doi: 10.1785/0120130309

Pagani, M., D. Monelli, G. Weatherill, L. Danciu, H. Crowley, V. Silva, P. Henshaw, L. Butler, M. Nastasi, L. Panzeri, M. Simionato, and D. Vigano, OpenQuake Engine: An Open Hazard (and Risk) Software for the Global Earthquake Model, Seismological Research Letters, May/June 2014, v. 85, p. 692-702, doi:10.1785/0220130087

Pagani, M., Monelli, D., Weatherill, G. A. and Garcia, J. (2014). The OpenQuake-engine Book: Hazard. Global Earthquake Model (GEM) Technical Report 2014-08, doi: 10.13117/-GEM.OPENQUAKE.TR2014.08, 67 pages.

Crowley H., Monelli D., Pagani M., Silva V., Weatherill G., (2015), OpenQuake Engine User Instruction Manual

Contact

Project lead	ETH Zürich
Project coordinator	Prof. Dr. Domenico Giardini
Project manager	Dr. Kauzar Saleh
Project office	ETH Department of Earth Sciences

Sonneggstrasse 5, NO H62, CH-8092 Zürich

sera_office@erdw.ethz.ch

+41 44 632 9690

Project website www.sera-eu.org

Liability claim

The European Commission is not responsible for any use that may be made of the information contained in this document. Also, responsibility for the information and views expressed in this document lies entirely with the author(s).